Upregulation of Indoleamine 2,3-Dioxygenase 1 in Tumor Cells and Tertiary Lymphoid Structures is a Hallmark of Inflamed Non–Small Cell Lung Cancer

Alban Bessede[1], Florent Peyraud[2], Sylvestre Le Moulec[3], Sophie Cousin[4], Mathilde Cabart[4], François Chomy[4], Christophe Rey[1], Oren Lara[1], Ophélie Odin[1], Imane Nafia[1], Jean-Philippe Guegan[1], and Antoine Italiano[2,4,5]

ABSTRACT

Purpose: Overexpression of the tryptophan-catabolizing enzyme indoleamine 2,3-dioxygenase 1 (IDO1) has been reported in several tumor types, including non–small cell lung cancer (NSCLC), and has been shown to promote tumor-immune evasion and inhibit T-cell activation through increased tryptophan degradation and the production of several immunosuppressive metabolites collectively known as kynurenines. However, it remains unclear whether IDO1 expression by tumor cells is detrimental specifically in the context of programmed cell death protein 1 (PD-1)/programmed death ligand 1 (PD-L1) axis blockade.

Experimental Design: We analyzed the transcriptome of 891 NSCLC tumor samples from patients enrolled in two large randomized clinical trials investigating the safety and activity of atezolizumab, a humanized IgG1 mAb that targets PD-L1, versus docetaxel in patients with advanced NSCLC. We complemented these transcriptomics results at the protein level by using multiplex immunofluorescence and at the functional level with *in vitro* experiments.

Results: The increased expression of the tryptophan-catabolizing enzyme IDO1 was significantly associated with improved objective response, progression-free survival, and overall survival in patients treated with PD-L1 inhibitors, but not in those treated with chemotherapy. Strikingly, inflamed tumors had higher levels of IDO1, and IDO1 was also expressed in tertiary lymphoid structures (TLS) by mature follicular dendritic cells. L-kynurenine impaired the differentiation of antibody-producing B cells induced by follicular helper T (Tfh)/B-cell interactions, a hallmark process within TLS.

Conclusions: IDO1 pathway in NSCLC is driven by the immune system rather than by tumor cells. Targeting IDO1 in combination with anti–PD-1/PD-L1 might be beneficial only in patients with inflamed tumors and particularly in those bearing TLS.

Introduction

Despite several attempts to reduce the consumption of tobacco, lung cancer remains the leading cause of cancer-related death. Eighty percent of patients with non–small cell lung cancer (NSCLC) are diagnosed with advanced disease in Western countries. The development of mAbs targeting programmed cell death 1 (PD-1) or its ligand programmed death ligand 1 (PD-L1) has revolutionized the management of patients with advanced NSCLC, with several studies demonstrating a significant impact in terms of objective response rate, progression-free survival (PFS), and overall survival (OS). Atezolizumab, an anti–PD-L1 mAb, was notably approved both for first-line treatment as a single agent in patients with NSCLC with high PD-L1 expression on tumor cells and/or intratumoral immune cells (1) or in combination with platinum-based chemotherapy combined with the VEGF inhibitor bevacizumab and for second-line treatment in all immune checkpoint inhibitor (ICI)-naïve patients (2).

However, most patients with advanced NSCLC display primary resistance to PD1/PD-L1 blockade, and the mechanisms involved in this phenomenon are still poorly understood (3).

Among the multiple mechanisms of primary resistance that have been proposed, some are related to tumor cell metabolism. In this regard, several findings suggest that the tryptophan-catabolizing enzyme indoleamine 2,3-dioxygenase 1 (IDO1; refs. 4, 5) may play a crucial role. IDO1 overexpression has been reported in several tumor types, including NSCLC, and IDO1 has been shown to promote tumor-immune evasion and inhibit T-cell activation by catabolizing tryptophan into several immunosuppressive metabolites, such as L-kynurenine (6–8). Decreased levels of tryptophan and increased expression of IDO1 were also found to be associated with an immunosuppressive tumor microenvironment composed notably of regulatory T cells (Tregs; refs. 9–11). However, it is unclear whether IDO1 expression by tumor cells specifically impacts the response to PD-1/PD-L1 blockade.

To decipher the effect of IDO1 expression on NSCLC patients' responses to immunotherapy, we first examined a comprehensive NSCLC gene expression dataset. This dataset comprises transcriptome profiles of 891 tumors obtained prior to treatment from the POPLAR study (phase II; ref. 12) and the OAK study (phase III; ref. 2). These studies, which compared the safety and efficacy of atezolizumab with the cytotoxic agent docetaxel in NSCLC, are among the largest worldwide. We then complemented this transcriptomic analysis with multiplex immunofluorescence (mIF) and digital pathology analyses to validate our findings at the protein level and to investigate the

[1]Explicyte, Bordeaux, France. [2]Department of Medicine, Institut Bergonié, Bordeaux, France. [3]Department of Medicine, Centre Hospitalier de Mont de Marsan, Mont de Marsan, France. [4]DITEP, Gustave Roussy, Villejuif, France. [5]Faculty of Medicine, University of Bordeaux, Bordeaux, France.

Corresponding Author: Antoine Italiano, Institut Bergonié, Bordeaux 33000, France. E-mail: a.italiano@bordeaux.unicancer.fr

Clin Cancer Res 2023;29:4883–93

doi: 10.1158/1078-0432.CCR-23-1928

Translational Relevance

A significant subgroup of non–small cell lung cancer (NSCLC) cases exhibit an inflamed phenotype but fail to respond to checkpoint immunotherapy. Our research reveals that tumors in these cases selectively express the immunosuppressive enzyme indoleamine-2,3-dioxygenase (IDO), both within the tumor cells and within tertiary lymphoid structures (TLS). Through mechanistic studies, we have demonstrated that IDO plays a role in limiting the antitumor immune activity of TLS. These findings suggest that patients with NSCLC with inflammatory tumor infiltrates and the presence of TLS are more likely to benefit from IDO inhibition.

correlation between the expression of IDO1 by tumor cells and the spatial distribution of $CD8^+$ T cells.

Materials and Methods

Patient population

Gene expression data were collected from patients included in the open-label, randomized phase II POPLAR (NCT01903993) and phase III OAK trials (NCT02008227), which evaluated atezolizumab versus docetaxel in patients with NSCLC who progressed following platinum-based chemotherapy (2, 12) and enrolled 287 and 1,225 patients, respectively. Patients in both trials received either 1,200 mg atezolizumab i.v. every 3 weeks until disease progression, loss of clinical benefit, or 75 mg/m^2 docetaxel i.v. every 3 weeks until progressive disease (PD). The POPLAR and OAK trials showed significant improvement in OS with atezolizumab versus docetaxel, regardless of PD-L1 expression (2, 12). No crossover was allowed, and OS was the primary endpoint.

mIF analysis was performed on tumor samples from patients included in an institutional molecular profiling program (BIP, sponsor: Institut Bergonié, Bordeaux, France, NCT02534649). The inclusion criteria were age ≥ 18 years, histologic confirmation of malignant tumor, unresectable and/or metastatic disease, at least one tumor evaluation by imaging after initial immunotherapy administration, and available paraffin-embedded tumor material obtained before initial immunotherapy administration.

Written informed consent was obtained from all the patients. The studies were conducted in accordance with Declaration of Helsinki.

RNA-sequencing data analysis

FASTQ files generated during the POPLAR (GO28753) and OAK (GO28915) clinical trials were downloaded from the European Genome-Phenome Archive (EGAC00001002120). Raw data were first processed through fastp software (v0.32.2) to remove reads containing adapters, poly-N sequences, and reads with low quality. Paired-end clean reads were mapped to the human reference genome (GRCh38 - Gencode release 39) and counted using STAR software (v2.7.10a). Differentially expressed genes were tested using the DESeq2 R package (v1.36.0), and gene signature enrichment analyses were performed using the fsgea R package (v1.22.0) with GO-BP terms. Immune cell estimations were performed, and tertiary lymphoid structure (TLS) signature scores were calculated by the ssGSEA framework using the consensusTME R package (v0.0.1.9) with the gene set by Bindea and colleagues (13) and Hennequin and colleagues (14), respectively. Patients were further classified as TLS-high or TLS-low based on the optimal cut-off point with PFS as the outcome (survminer R package V.0.4.9). To impute the PD-L1 status for all the patients treated with atezolizumab, an optimal cut-off point was defined to classify the patients as PD-L1-high (≥1%) or PD-L1-low (<1%) using the cutpointr R package (v1.1.2), and the maximize metric method was used for the patients with PD-L1 22C3 measurements. ROC curves and volcano plots were drawn using the ROCit R package (v2.1.1) and Enhanced Volcano R package (v1.14.0), respectively.

Single-cell RNA-sequencing data analysis

Processed data and metadata from the single-cell RNA sequencing (scRNAseq) of tonsillar stromal cells were downloaded from the Gene Expression Omnibus database (GSE173539). The data were normalized using global-scaling normalization in Seurat (v4.3.0), and $CD23^+$ FDC cells were identified using a FCER2 gene expression cutoff of 1.5.

Spatial transcriptomic data analysis

Spatial transcriptomic data were acquired as previously described (15). In brief, tumor slides from 6 patients were analyzed on the Nanostring GeoMX Digital Spatial Profiler platform using the Whole Transcriptome Atlas panel (NanoString). Regions of interest were drawn on the TLS structures, which were further segmented into $CD20^+$ and $CD20^-$ areas of interest (AOI). Raw counts were normalized using full quantile normalization from the limma R package (v3.52.4), and the estimation of Treg and pDC abundances was performed using the SpatialDecon R package (v1.6.0) and safeTME data as a cell-profile matrix.

TLS and immune phenotype assessment

TLS and tumor-immune phenotypes were defined by expert pathologists. TLS were defined as aggregates of $CD20^+$ and $CD3^+$ cells (composed of at least 50 cells) located within the tumor or a maximum of 1 mm from the tumor edges. The tumor-immune phenotype was defined according to the localization of $CD8^+$ T cells within the tumor specimen. The "inflamed" profile was characterized by the presence of $CD8^+$ T cells within the tumor parenchyma, the "excluded" profile was characterized by the presence of $CD8^+$ T cells that were mainly located in the stroma surrounding the nest of tumor cells, and the "desert" profile was characterized by an extreme paucity or absence of T cells in either the parenchyma or the stroma of the tumor.

mIF and IHC

IHC and mIF analyses were performed on the automated Ventana Discovery XT staining platform (Ventana Medical Systems). In brief, slides of tumor tissue were deparaffinized, and antigen retrieval was performed by heat-induced epitope retrieval using standard CC1 reagent (Tris-based buffer, pH 8.0; Ventana Medical Systems). The slides were then incubated with primary antibodies against the following molecules, according to panel composition: CD8 (C8/144B, Dako: Agilent Technologies), CD4 (SP35, Ventana), Foxp3 (236 A/E7, Abcam), CD20 (L26, Ventana), CD3 (2GV6, Ventana), CD11c (D3V1E, Cell Signaling Technology, 1/400), CD14 (EPR3653, Cell Marque), CD21 (2G9, Cell Marque), CD23 (SP23, Ventana), CD163 (10D6, Novocastra), IDO1 (UMAB126, Origene), Ki67 (30–9, Ventana), PanCK (AE1/AE3/PCK26, Ventana), Mum1 (EP190, Cell Marque), PD-1 (NAT105, Cell Marque) and PD-L1 (QR-1, Diagomics).

Bound primary antibodies were detected using OmniMap HRP-conjugated anti-rabbit IgG (760–4311; Ventana; Roche) or OmniMap HRP-conjugated anti-mouse IgG (760–4310; Ventana; Roche), followed by tyramide signal amplification using opal fluorophores

(Opal 480, Opal 520, Opal 570, Opal 620, Opal 690 and/or Opal 780; Akoya Biosciences) for mIF or DISCOVERY Purple or a 3,3′-diaminobenzidine (DAB) chromogen detection kit (Roche) for IHC. The slides were ultimately counterstained with either spectral 4′,6-diamidino-2-phenylindol (Akoya Biosciences) or hematoxylin (Roche), cover-slipped, and digitized using a multispectral imaging platform (PhenoImager HT, Akoya).

The multispectrally acquired images were unmixed using spectral libraries previously built from images stained for each fluorophore (monoplex) and with inForm Advanced Image Analysis software (inForm v.2.60; Akoya Biosciences). Tumor areas of each tissue slide were delineated by a pathologist using PhenoChart (Akoya Biosciences), and the annotated sections were analyzed using inForm software (v.2.6.0). Tissues were first segmented into "tumor" versus "stroma" areas based on PanCK staining, and cells were segmented on the basis of DAPI and fluorescent membrane signals. Mean fluorescent marker intensities for each cell were extracted, and signal intensities were normalized using the GaussNorm function from the flowStats R package (v4.8.2). Cells were ultimately phenotyped using a thresholding method in FlowJo software (v.10.8.0; FlowJo). Intercellular distances between $PanCK^+$ and $CD8^+$ cells were computed using the PhenoptReport (v0.3.2) R package.

T-cell killing assay

Peripheral blood mononuclear cells (PBMC) were isolated from whole blood of healthy donors (Etablissement Français du Sang – EFS, Bordeaux) using density-gradient centrifugation with Lymphoprep (STEMCELL Technologies) per the manufacturer's instructions and cryopreserved.

H1299 lung cancer cells stably expressing the NucLight Red probe were maintained in RPMI1640 medium with 10% FBS. Cells (2.5×10^4) were seeded in 96-well plates and incubated for 24 hours to reach 30% confluency. Cells were then cocultured with PBMC (ratio tumor:PBMC 1:5) for 120 hours at 37°C in the IncuCyte ZOOM Live-Cell Analysis System (Sartorius) and were treated with anti-CD3 antibody (0.3 or 3 μg/mL), L-kynurenine (10 or 100 μmol/L) and 1× IncuCyte caspase-3/7 dyes (Sartorius) in complete medium or not treated.

To analyze the induction of apoptosis, treated plates were analyzed every 3 hours. Phase contrast, green channel (fluorescent caspase3/7 apoptosis probe), and red channel (fluorescent tumor nuclear probe) images were acquired on an IncuCyte ZOOM Live cell imager using a 10x objective. Image analysis was performed using IncuCyte ZOOM software after a segmentation mask was applied on phase contrast images to identify the cell surface, on red fluorescence images to select tumor cells (expressing the red fluorescent nuclear probe), and on green fluorescence images to identify apoptotic cells (caspase 3/7 probe; DEVD-NucView488). Overlay segmentation analysis was performed to identify apoptotic tumor cells. Data were analyzed and plotted using Graph Pad Prism v9.1.0 software. In addition, 120 hours following coculture initiation and treatment, supernatants were collected, and the effects of L-kynurenine on T-cell activation were evaluated through the quantification of IFNγ release by HTRF measurement on a Spark multimode microplate reader (Tecan) using the Human IFN Gamma Kit (Cisbio).

Ex vivo human follicular helper T/human B-cell coculture assay

Minced tonsils were dissociated using collagenase D (0.5 mg/mL) and DNAse I (100 U/mL) on the GentleMACS Dissociation System (Miltenyi Biotec) for 30 minutes at 37°C. After washing, the cells were cryopreserved in cryostor CS10. Memory B cells were isolated from thawed tonsillar cells using the EasySep Human Memory B-Cell Isolation Kit (StemCell) according to the manufacturer's instructions. To isolate follicular helper T (Tfh) cells, $CD4^+$ T cells were first isolated from cryopreserved tonsils and then incubated with anti-CXCR5-biotin antibody (REA103, BioLegend). $CD4^+CXCR5^+$ cells were isolated using the EasySep Release Human Biotin Positive Selection Kit (StemCell). The purity (75%–90%) of Tfh and memory B cells was validated by flow cytometry.

Memory B cells and Tfh cells were seeded in 96-well plates in complete medium and treated with SEB and L-kynurenine (10, 30, 100 μmol/L) or not treated. After 6 days, supernatants were collected, and soluble IgG was quantified using the Human IgG HTRF kit (Cisbio) according to the manufacturer's instructions.

Survival and statistical analyses

Wilcoxon and χ^2 tests were used where indicated. For survival analyses, the log-rank test was used to compare Kaplan–Meier survival curves (survival R package v3.3.1). The Cox proportional hazards regression model was used to estimate HR and 95% confidence intervals (CI). Patients were classified as IDO1-high or IDO1-low based on an optimized threshold obtained using the maximally selected rank statistics from the maxstat R package and using PFS as the optimal outcome (survminer R package v0.4.9). TLS^+ patients were classified as TLS IDO1-high or TLS IDO1-low if they displayed at least one TLS with 10% $IDO1^+$ cells. Multivariable Cox proportional hazards regression models were used to compare the interdependence of distinct biomarkers for the prediction of ICI benefit (survivalAnalysis R package v0.3.0). All analyses were conducted using R v.4.2.1.

Data availability

Raw and processed transcriptomic data and limited clinical data have been deposited at the European Genome-phenome Archive (EGA), which is hosted by the EBI and the CRG, under accession number EGA: EGAS00001005013. Additional clinical data are available via request from https://vivli.org/ourmember/roche/. The immunofluorescence datasets are not publicly available due to information that could compromise research participant consent. According to French/European regulations, any reuse of the data must be approved by the ethics committee. Each request for access to the immunofluorescence dataset (including the images) will be granted after a request is sent to the corresponding author (A. Italiano) and approval by the ethics committee.

Results

IDO1 expression is independently associated with improved outcome in patients treated with atezolizumab

We first investigated the impact of *IDO1* gene expression on the PFS of patients treated with atezolizumab. As shown in **Fig. 1A**, the PFS of patients with high expression of IDO1 was significantly higher than that of patients with low expression [median, 3.8 (2.8–4.2) vs. 1.89 (1.5–2.7) months, $P < 0.001$]. Strikingly, high IDO1 expression was also associated with improved OS (**Fig. 1B**) and a higher objective response (**Fig. 1C**). None of these correlations were observed in the docetaxel arm (**Fig. 1D–F**), suggesting a predictive value of IDO1 gene expression specifically for response to atezolizumab. Other factors associated with PFS and OS in patients treated with atezolizumab in the univariate analysis were histological subtype (adenocarcinoma vs. squamous cell cancer), PD-L1 expression, and increased tertiary lymphoid structure (TLS) signatures (Supplementary Fig. S1). In

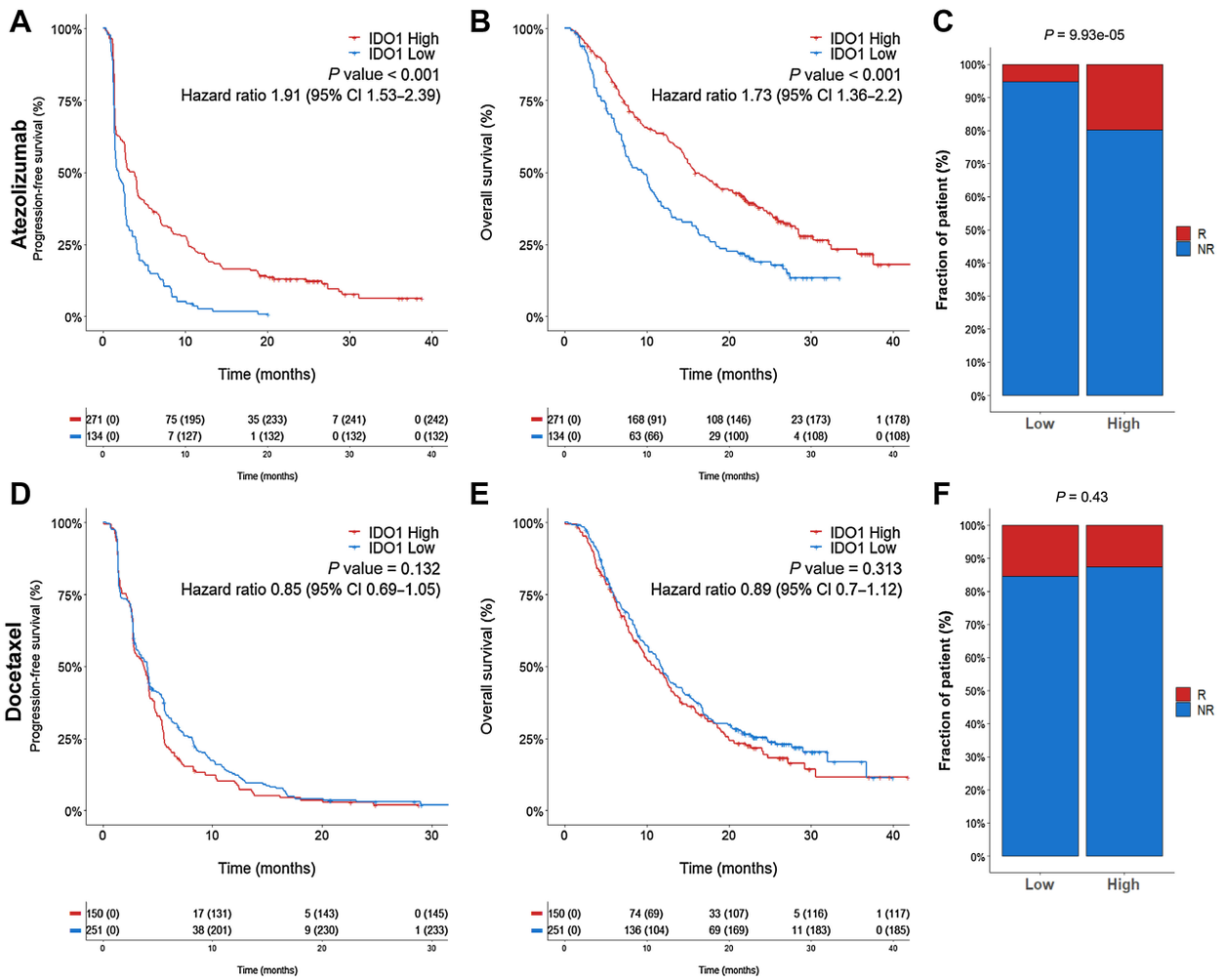

Figure 1.

High IDO1 expression is associated with a favorable response to ICI. **A–E,** Patients from the POPLAR and OAK trials were classified as high or low based on their baseline level of *IDO1* gene expression as assessed by RNA-seq. Kaplan–Meier curves of the progression-free survival (**A–D**) and overall survival (**B–E**) of patients treated with atezolizumab (**A** and **B**) or docetaxel (**D** and **E**). **C–F,** Proportion of patients treated with atezolizumab (**C**) or docetaxel (**F**) with high and low expression of IDO1 who responded to treatment (NR, nonresponders; R, responders). The *P* values were calculated using a χ^2 test.

multivariate analysis, high IDO1 expression remained independently associated with PFS and OS (Supplementary Table S1).

IDO1 expression is upregulated in inflamed NSCLC

Given the positive correlation between IDO1 expression and outcome of patients treated with immunotherapy, we reasoned that IDO1 expression may be a surrogate for an inflamed tumor microenvironment. Previous studies have suggested a positive correlation between high IDO1 and PD-L1 expression in the tumor microenvironment (TME), which appears to be mediated by $CD8^+$ T cells (6). We therefore analyzed the correlation between IDO1 and PD-L1 and found a significant positive correlation, as illustrated in **Fig. 2A** and **B**. Gene Ontology–Biological Process (GO–BP) enrichment analysis revealed that several immune pathways, such as the B-cell receptor and T-cell receptor signaling pathways, as well as immune response-regulating pathways, were enriched in the group with high IDO1 expression (**Fig. 2C** and **D**). By using a deconvolution approach, we also found that the TME composition differed significantly between IDO1-high and IDO1-low tumors. IDO1-high tumors were characterized by the highest expression of genes specific to immune cell populations such as IFNγ-producing Th1 cells, $CD8^+$ T cells, natural killer cells, cytotoxic lymphocytes, and B cells (**Fig. 2E**).

We complemented this transcriptional approach by performing mIF analysis with a 7-color panel (CD8/CD163/IDO1/PD1/PD-L1/PanCK) on an independent series of 53 NSCLC tumors treated with ICI and included in an institutional molecular-profiling program (Bergonie Institute Profiling, BIP, NCT02534649) (Supplementary Fig. S2). The characteristics of these patients are presented in Supplementary Table S2. As previously described (16), $CD163^+$ tumor macrophages were found to be associated with a poor prognosis in NSCLC, whereas tumor PD-L1 expression and stromal

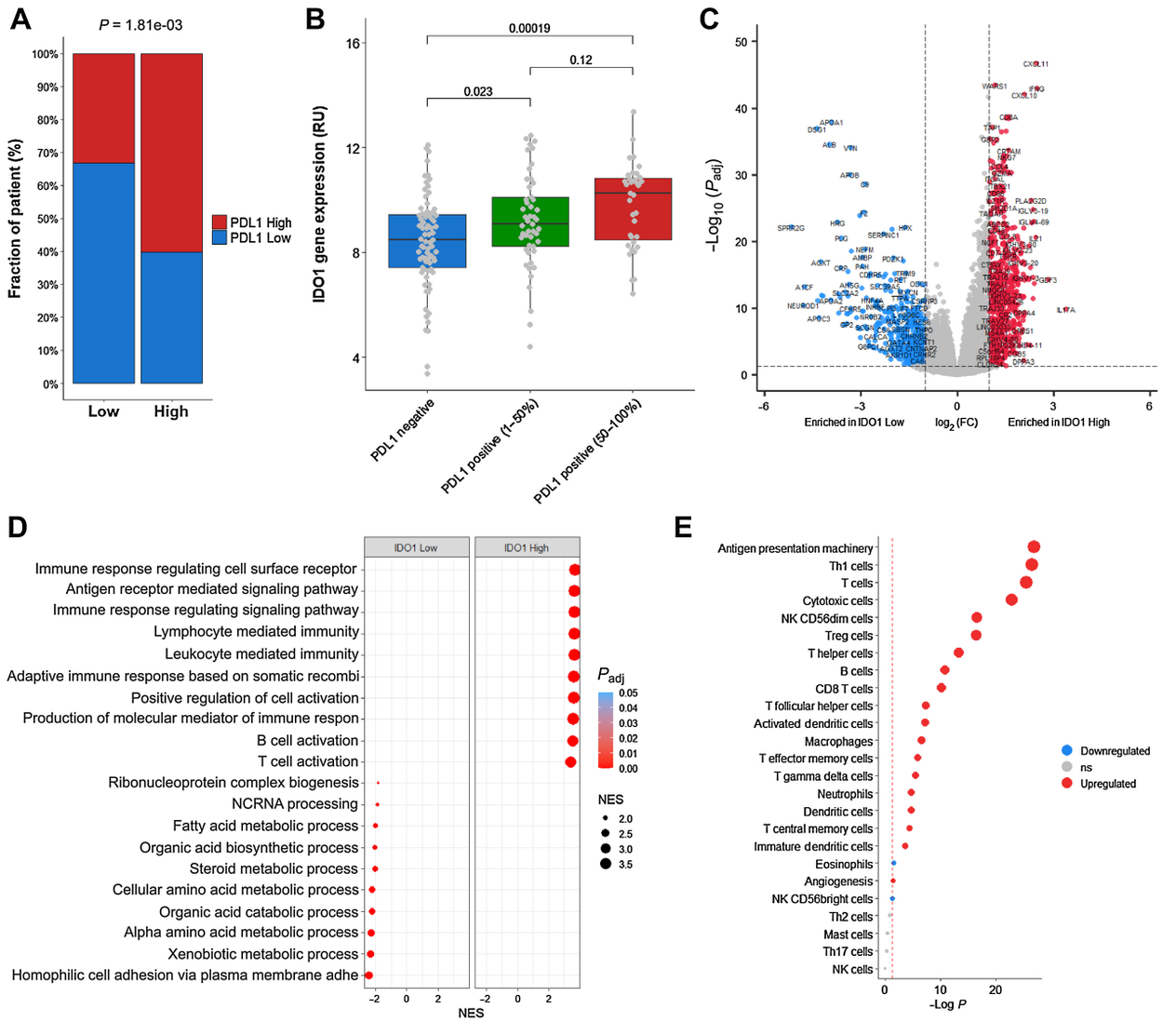

Figure 2.

High IDO1 expression is associated with the inflammatory response. **A,** Atezolizumab-treated patients from the POPLAR and OAK trials were classified as *IDO1*-high or *IDO1*-low based on their baseline level of *IDO1* gene expression and PDL1-high (≥1%) or PDL1-low (<1%) based on their PD-L1 22C3 assay status. The *P* value was calculated using a χ^2 test. **B,** Histogram of *IDO1* gene expression levels (normalized counts) according to the PDL1 22C3 assay. The *P* values were calculated using the Wilcoxon test. **C,** Volcano plot showing the differentially expressed gene between IDO1-high and IDO1-low patients. **D,** Gene ontology analysis of the differentially expressed genes between IDO1-high and IDO1-low patients. NES, normalized enrichment score. **E,** Assessment of the immune microenvironment of patients with high and low IDO1 gene expression by data deconvolution using Bindea et al. gene sets. Bubble plot of the genes upregulated (red dots) and downregulated (blue dots) in patients with high IDO1 expression. The *P* values were calculated using the Wilcoxon test.

infiltration by $CD8^+$ cells were found to be correlated with a better outcome (Supplementary Fig. S3). IDO1 expression by tumor cells was also associated with a trend toward higher long-term clinical benefit (36.4% vs. 15%, $P = 0.09$) and with significantly improved PFS [median, 5.3 (3.8–NA) vs. 3.3 (2.3–6.1) months, $P = 0.036$] (**Fig. 3A** and **B**). IDO1 expression by tumor cells was also correlated with a higher infiltration of activated $CD8^+$ cells, defined as $CD8^+/PD1^+$, in both the stroma and tumor of IDO1-high patients (**Fig. 3C** and **D**). Moreover, the abundance of IDO1-expressing tumor cells was significantly correlated with the immune contexture, with a gradual increase in IDO1 expression by tumor cells from desert to inflamed tumors (Supplementary Fig. S4). Analysis of the spatial distribution of immune cells in the tumor microenvironment showed that the median distance between $PanCK^+$ tumor cells and the nearest $CD8^+$ cell was significantly higher in IDO1-low tumors than in IDO1-high tumors (**Fig. 3E** and **F**), thus confirming the proximity of $CD8^+$ T cells to tumor cells in IDO1-high tumors.

Through studies depleting tryptophan and limiting the production of metabolites such as L-kynurenine, IDO1 activity has been linked

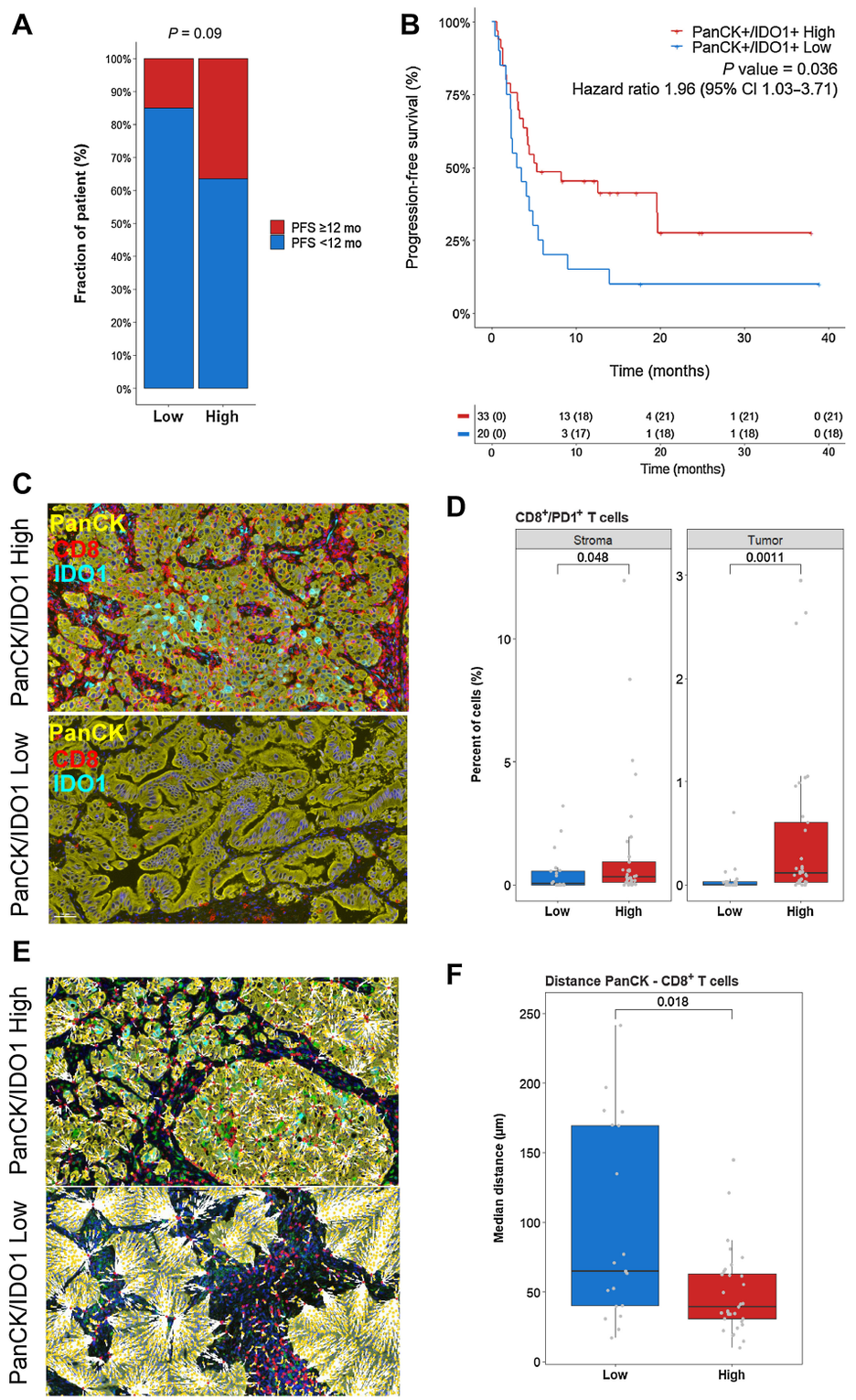

Figure 3.
Tumor expression of IDO1 is associated with increased CD8$^+$ T-cell infiltration. **A,** Proportion of patients with high and low percentages of PanCK$^+$/IDO1$^+$ cells according to progression-free survival. The *P* value was calculated using a χ^2 test. **B,** Kaplan–Meier curves of the progression-free survival of patients classified as high or low based on levels of PanCK$^+$/IDO1$^+$ cells. **C,** CD8$^+$ T-cell infiltration in patients with high and low expression of IDO1 in PanCK$^+$ cells. **D,** Histograms of the percentage of activated CD8$^+$/PD-1$^+$ cells in the stroma and tumor areas of patients with high and low PanCK$^+$/IDO1$^+$ cell levels. The *P* values were calculated using Wilcoxon tests. **E,** Nearest distances between PanCK$^+$ and CD8$^+$ cells in patients with high and low levels of PanCK$^+$/IDO1$^+$ cells. The minimum intercellular distance is shown by a white dashed segment. **F,** Histogram of the median distance between PanCK$^+$ and CD8$^+$ cells in patients with high and low levels of PanCK$^+$/IDO1$^+$ cells. The *P* value was calculated using Wilcoxon tests.

to impaired CD8$^+$ T-cell functions, including decreased cell proliferation and defects in cytotoxic granule production (17, 18). By incubating H1299 lung cancer cells with (PBMCs originating from healthy donors), we observed T-cell–mediated tumor cell apoptosis upon anti-CD3 antibody treatment, which was inhibited in a dose-dependent manner by L-kynurenine exposure (Supplementary Fig. S5A and S5B). A concomitant decrease in T-cell activation, as reflected by the inhibition of IFNγ secretion, was also observed. Altogether, these

results demonstrate that IDO1 is expressed in inflamed tumors and might participate in a negative feedback loop to exert immunosuppressive effects.

IDO1 is expressed in mature follicular dendritic cells in TLS and restricts B-cell activation

Interestingly, in addition to expression by tumor cells, we also observed the expression of IDO1 in TLS (Supplementary Fig. S6). We have recently reported that the presence of mature TLS is a strong predictor of outcome in patients with NSCLC treated with ICI (19). Mature TLS are composed of prominent B-cell follicles and follicular dendritic cells (FDC) that are adjoined to a smaller T-cell zone containing a mixture of $CD4^+$ and $CD8^+$ T cells (20). To decipher the pattern of IDO1 expression in TLS, we developed an additional multiplex 9-color panel (CD3/CD11c/CD14/CD20/CD21/CD23/IDO1/Mum1/DAPI) to identify the main cell subtype expressing IDO1. As shown in **Fig. 4**, IDO1 was mainly expressed by FDC, specifically by $CD20^-/CD21^+/CD23^+$ cells, and this expression was consistent in almost all the TLS analyzed (**Fig. 4A** and **B**). Analysis of scRNAseq data from tonsillar stromal cells also confirmed that IDO1 was expressed by $CD23^+$ FDC (**Fig. 4C**). We then investigated the impact of IDO1 expression within TLS and observed that TLS IDO-high patients were more likely to have a poor clinical outcome than TLS IDO-low patients [median PFS, 4.7 (3.1–NA) vs. 19.7 (3.8 vs. NA), $P = 0.27$; **Fig. 4D**)].

TLS promote B-cell maturation into plasma cells and antibody production, which is associated with the response to immunotherapy (20, 21). We reasoned that IDO expression by mature DC may have a detrimental effect within TLS by impairing Tfh-mediated B-cell differentiation into antibody-secreting cells. We thus used an *ex vivo* coculture assay with Tfh cells and memory B cells isolated from human tonsils to investigate the impact of IDO1 activity on B-cell activation by Tfh cells through the addition of L-kynurenine. As shown in **Fig. 4E**, coculture of memory B cells with activated Tfh cells led to the secretion of IgG, which was inhibited in a dose-dependent manner upon L-kynurenine treatment.

IDO1 expression in TLS is associated with pDC and Treg levels

IDO1 expressed by DC has been shown to regulate tolerance by activating Tregs or by inducing $CD4^+$ T-cell differentiation into "inducible" Tregs (22–25). As we previously showed that Treg presence within TLS correlates with a worse response rate in ICI-treated patients with TLS^+ sarcoma (15), we decided to investigate whether the level of IDO1 expression correlates with Treg infiltration within TLS. By reanalyzing our spatial transcriptomics data, we found that TLS with high expression of IDO1 also had higher levels of plasmacytoid DC and Tregs (**Fig. 5A** and **B**). We thus analyzed the correlation between IDO1 expression and Treg presence inside the TLS of patients with NSCLC with 2 mIF panels consisting of the following markers: CD4/CD8/Foxp3/Ki67/CD20/DAPI and CD21/CD23/IDO1/CD3/CD20/DAPI (**Fig. 5C**). As shown in **Fig. 5D**, higher IDO1 expression inside TLS was associated with an increased proportion of proliferating Tregs ($CD4^+/Foxp3^+/Ki67^+$ cells). The presence of these cells was further correlated with lower response to ICI (**Fig. 5E**) and poor outcome (**Fig. 5F** and **G**).

Discussion

Our results indicate that immune-infiltrated NSCLC is characterized by strong expression of IDO1 and PD-L1 by tumor cells. In line with previous observations in melanomas (26), our data strongly suggest that the induction of these immunosuppressive mechanisms is elicited by an inflammatory context rather than by the tumor cells themselves, and these mechanisms could serve as negative feedback for inflammation resolution.

We and others have recently reported that the level of B cells and TLS gene signatures are predictive of outcomes in patients with sarcoma and melanoma treated with ICI (27–29). By using a pathological assessment approach in three independent cohorts encompassing 11 tumor types, we demonstrated that TLS status (as assessed in paraffin-embedded samples) is a robust and reproducible predictor of outcome in patients treated with ICI, and this association was independent of PDL1 or CD8 expression status (19). We further confirmed the consistency of this biomarker in identifying responders in study populations from clinical trials investigating immunotherapy regimens (15).

In addition to expression in tumor cells, we also observed the expression of IDO1 in TLS. By comparing the gene expression profile of TLS-positive versus TLS-negative Merkel cell carcinoma, Nakamura and colleagues (30) showed overexpression of IDO1 in the tumors of TLS-positive samples. Our study is the first to report the expression of IDO1 within TLS. By using an mIF approach, we demonstrated that IDO1 was mainly expressed by mature DC ($CD23^+$), which play an important role in antigen presentation to T cells. IDO1 participates in one crucial mechanism by which DC promote tolerance (23, 31) by suppressing effector T cells and promoting Tregs. Strikingly, we found that IDO1 expression inside TLS was significantly associated with an increased proportion of proliferating Tregs and lower clinical benefit of ICI.

To support the functional impact of IDO1 expression within TLS that we identified, we conducted an *ex vivo* coculture assay using circulating Tfh cells and B cells isolated from human tonsils. The cooperation between these cell types in mature TLS is a key element of anticancer immunity (20). Interestingly, we found that L-kynurenine, the main bioactive catabolite of IDO1 and used here to mimic IDO activity, impaired B-cell antibody secretion, mediated by physiologic support from Tfh cells.

Even if TLS presence is a robust predictor of ICI efficacy, not all patients with TLS-positive tumors achieve a benefit from treatment in the clinic. The induction of the IDO pathway within TLS structures may thus be part of a feedback loop that dampens TLS immune activity, making the IDO pathway a potential therapeutic target to reinvigorate TLS-driven antitumor immunity.

High expression of IDO1 by tumor cells was independently associated with outcome in patients with NSCLC treated with immunotherapy but not in patients treated with chemotherapy, indicating that high expression of IDO1 is not prognostic per se but a surrogate of increased tumor-immune cell infiltration/activity and therefore predictive of a higher probability of response to immune checkpoint inhibition. To date, clinical data regarding the impact of IDO1 inhibition in NSCLC are limited. In a phase I study investigating the IDO1-specific inhibitor epacadostat in combination with atezolizumab for patients with previously treated advanced NSCLC that enrolled 29 patients, only one patient had an objective response (32). However, this study included all-comers, and analysis of the tumor samples revealed that most enrolled patients lacked baseline PD-L1 expression (PD-L1 expression <1% in tumor and immune cells) and had cold tumors. Our current results suggest that IDO inhibitor efficacy might be restricted to patients with a T-cell–inflamed tumor microenvironment and/or TLS. Combining IDO1 inhibitors with ICI may result in synergistic

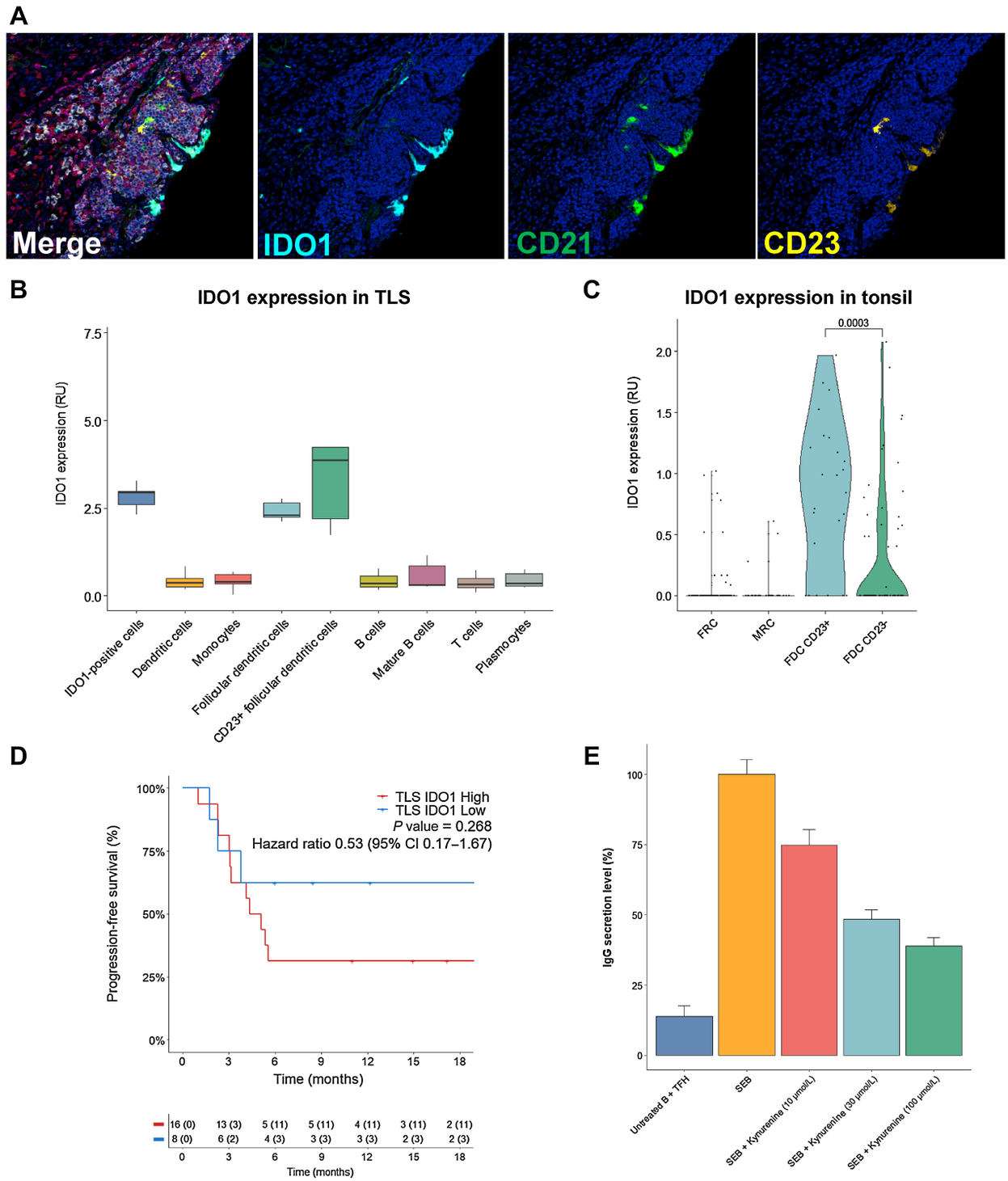

Figure 4.

IDO1 is expressed on CD21$^+$/CD23$^+$ FDC within TLS and restricts B-cell activation. **A,** Representative image from the CD11c/CD14/CD3/CD20/CD21/CD23/IDO1/-Mum1/DAPI multiplex immunofluorescence panel focused on a TLS from an NSCLC adenocarcinoma section. **B,** IDO1 expression in the different cell subsets identified within TLS (n = 6 patients). **C,** scRNAseq analysis of IDO1 expression in different tonsillar stromal cell subsets (GSE173539). **D,** Kaplan–Meier curves of the progression-free survival of TLS$^+$ patients classified as TLS IDO-positive or TLS IDO-negative (positive = at least one TLS with 10% IDO1+ cells). **E,** Level of IgG secretion by B-cell and Tfh cell cocultures activated with SEB (1 ng/mL) for 7 days or not treated; the doses of kynurenine are indicated (n = 2 different donors).

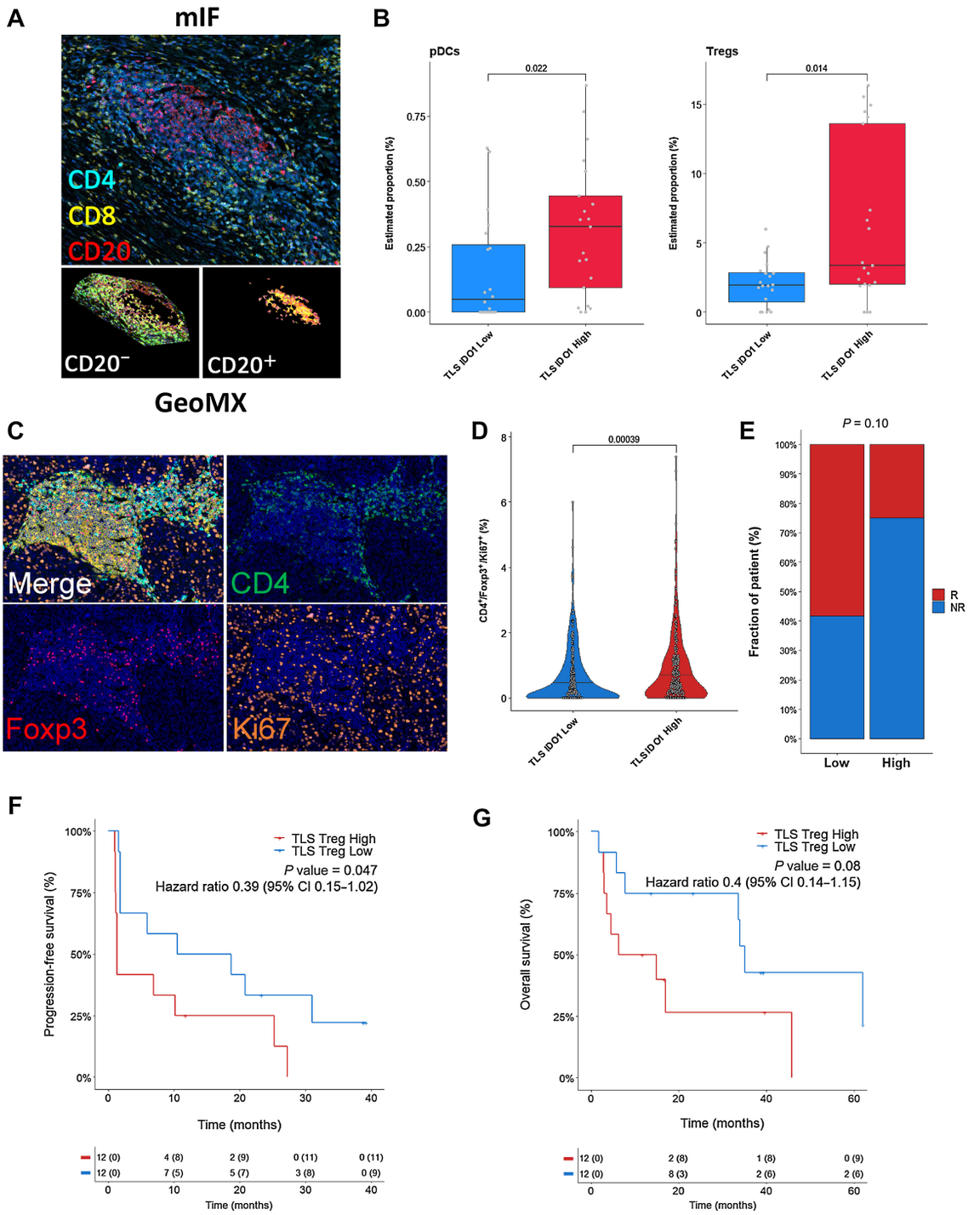

Figure 5.

IDO1 expression in TLS correlates with increased Treg levels and poor prognosis. **A,** Representative illustration of a GeoMx DSP-analyzed TLS. CD4/CD8/CD20 multiplex IF staining (top) and CD20 segmentation masks (bottom) for GeoMx transcriptomics analysis. **B,** Estimation of the percentage of pDC (left) and Tregs (right) in the CD20 areas of TLS expressing high or low levels of IDO1 by SpatialDecon analysis of GeoMx data. **C,** Representative image from the CD4/CD8/CD20/Ki67/Foxp3/DAPI multiplex immunofluorescence panel focused on a TLS from an NSCLC adenocarcinoma section. **D,** Proportion of proliferating Tregs ($CD4^+/Foxp3^+/Ki67^+$) in TLS according to IDO1 expression. The analyzed TLS ($n = 528$) were classified as high or low based on the median IDO1 expression level inside TLS. The *P* value was calculated using a Wilcoxon test. **E,** Proportion of patients with high and low levels of proliferating Tregs in TLS according to their response to ICI. The *P* value was calculated using a χ^2 test. **F** and **G,** Kaplan–Meier curves of the progression-free survival (**C**) and overall survival of patients classified as high and low according to the levels of proliferating Tregs ($CD4^+/Foxp3^+/Ki67^+$) in TLS.

activity and further improve response rates in this specific group of patients.

Authors' Disclosures

A. Bessede reports other support from Explicyte outside the submitted work. C. Rey is an employee of Explicyte. O. Lara reports other support from Immusmol outside the submitted work. O. Odin reports other support from Immusmol outside the submitted work. J. Guégan is an employee of Exlicyte. A. Italiano reports grants from Roche outside the submitted work. No disclosures were reported by the other authors.

Authors' Contributions

A. Bessede: Conceptualization, data curation, writing–review and editing. **F. Peyraud:** Data curation, writing–review and editing. **S. Le Moulec:** Investigation, writing–review and editing. **S. Cousin:** Investigation, writing–review and editing. **M. Cabart:** Investigation, writing–review and editing. **F. Chomy:** Investigation, writing–review and editing. **C. Rey:** Investigation, writing–review and editing. **O. Lara:** Investigation, writing–review and editing. **O. Odin:** Investigation, writing–review and editing. **I. Nafia:** Investigation, writing–review and editing. **J.-P. Guegan:** Data curation, formal analysis, investigation, methodology, writing–original draft, writing–review and editing. **A. Italiano:** Conceptualization, resources, supervision, funding acquisition, validation, investigation, writing–original draft, writing–review and editing.

Acknowledgments

This study was funded by Conseil Regional de Nouvelle-Aquitaine (grant BIP AIRIC)

The publication costs of this article were defrayed in part by the payment of publication fees. Therefore, and solely to indicate this fact, this article is hereby marked "advertisement" in accordance with 18 USC section 1734.

Note

Supplementary data for this article are available at Clinical Cancer Research Online (http://clincancerres.aacrjournals.org/).

Received June 26, 2023; revised July 28, 2023; accepted September 21, 2023; published first September 26, 2023.

References

1. Herbst RS, Giaccone G, de Marinis F, Reinmuth N, Vergnenegre A, Barrios CH, et al. Atezolizumab for first-line treatment of PD-L1-selected patients with NSCLC. N Engl J Med 2020;383:1328–39.
2. Rittmeyer A, Barlesi F, Waterkamp D, Park K, Ciardiello F, von Pawel J, et al. Atezolizumab versus docetaxel in patients with previously treated non-small-cell lung cancer (OAK): a phase 3, open-label, multicentre randomised controlled trial. Lancet 2017;389:255–65.
3. Camidge DR, Doebele RC, Kerr KM. Comparing and contrasting predictive biomarkers for immunotherapy and targeted therapy of NSCLC. Nat Rev Clin Oncol 2019;16:341–55.
4. Mellor AL, Munn DH. IDO expression by dendritic cells: tolerance and tryptophan catabolism. Nat Rev Immunol 2004;4:762–74.
5. Holmgaard RB, Zamarin D, Munn DH, Wolchok JD, Allison JP. Indoleamine 2,3-dioxygenase is a critical resistance mechanism in antitumor T cell immunotherapy targeting CTLA-4. J Exp Med 2013;210:1389–402.
6. Mandarano M, Bellezza G, Belladonna ML, Van den Eynde BJ, Chiari R, Vannucci J, et al. Assessment of TILs, IDO-1, and PD-L1 in resected non-small cell lung cancer: an immunohistochemical study with clinicopathological and prognostic implications. Virchows Arch 2019;474:159–68.
7. Schafer CC, Wang Y, Hough KP, Sawant A, Grant SC, Thannickal VJ, et al. Indoleamine 2,3-dioxygenase regulates anti-tumor immunity in lung cancer by metabolic reprogramming of immune cells in the tumor microenvironment. Oncotarget 2016;7:75407–24.
8. Smith C, Chang MY, Parker KH, Beury DW, DuHadaway JB, Flick HE, et al. IDO is a nodal pathogenic driver of lung cancer and metastasis development. Cancer Discov 2012;2:722–35.
9. Witkiewicz A, Williams TK, Cozzitorto J, Durkan B, Showalter SL, Yeo CJ, et al. Expression of indoleamine 2,3-dioxygenase in metastatic pancreatic ductal adenocarcinoma recruits regulatory T cells to avoid immune detection. J Am Coll Surg 2008;206:849–54.
10. Ino K, Yamamoto E, Shibata K, Kajiyama H, Yoshida N, Terauchi M, et al. Inverse correlation between tumoral indoleamine 2,3-dioxygenase expression and tumor-infiltrating lymphocytes in endometrial cancer: its association with disease progression and survival. Clin Cancer Res 2008;14:2310–7.
11. Mezrich JD, Fechner JH, Zhang X, Johnson BP, Burlingham WJ, Bradfield CA. An interaction between kynurenine and the aryl hydrocarbon receptor can generate regulatory T cells. J Immunol 2010;185:3190–8.
12. Fehrenbacher L, Spira A, Ballinger M, Kowanetz M, Vansteenkiste J, Mazieres J, et al. Atezolizumab versus docetaxel for patients with previously treated non-small-cell lung cancer (POPLAR): a multicentre, open-label, phase 2 randomised controlled trial. Lancet 2016;387:1837–46.
13. Bindea G, Mlecnik B, Tosolini M, Kirilovsky A, Waldner M, Obenauf AC, et al. Spatiotemporal dynamics of intratumoral immune cells reveal the immune landscape in human cancer. Immunity 2013;39:782–95.
14. Hennequin A, Derangère V, Boidot R, Apetoh L, Vincent J, Orry D, et al. Tumor infiltration by Tbet+ effector T cells and CD20+ B cells is associated with survival in gastric cancer patients. Oncoimmunology 2016;5:e1054598.
15. Italiano A, Bessede A, Pulido M, Bompas E, Piperno-Neumann S, Chevreau C, et al. Pembrolizumab in soft-tissue sarcomas with tertiary lymphoid structures: a phase 2 PEMBROSARC trial cohort. Nat Med 2022;28:1199–206.
16. Larroquette M, Guegan J-P, Besse B, Cousin S, Brunet M, Le Moulec S, et al. Spatial transcriptomics of macrophage infiltration in non-small cell lung cancer reveals determinants of sensitivity and resistance to anti-PD1/PD-L1 antibodies. J Immunother Cancer 2022;10:e003890.
17. Liu H, Liu L, Liu K, Bizargity P, Hancock WW, Visner GA. Reduced cytotoxic function of effector CD8+ T cells is responsible for indoleamine 2,3-dioxygenase-dependent immune suppression. J Immunol 2009;183:1022–31.
18. Frumento G, Rotondo R, Tonetti M, Damonte G, Benatti U, Ferrara GB. Tryptophan-derived catabolites are responsible for inhibition of T and natural killer cell proliferation induced by indoleamine 2,3-dioxygenase. J Exp Med 2002;196:459–68.
19. Vanhersecke L, Brunet M, Guégan J-P, Rey C, Bougouin A, Cousin S, et al. Mature tertiary lymphoid structures predict immune checkpoint inhibitor efficacy in solid tumors independently of PD-L1 expression. Nat. Cancer 2021;2:794–802.
20. Fridman WH, Meylan M, Petitprez F, Sun C-M, Italiano A, Sautès-Fridman C. B cells and tertiary lymphoid structures as determinants of tumour immune contexture and clinical outcome. Nat Rev Clin Oncol 2022;19:441–57.
21. Meylan M, Petitprez F, Becht E, Bougoüin A, Pupier G, Calvez A, et al. Tertiary lymphoid structures generate and propagate anti-tumor antibody-producing plasma cells in renal cell cancer. Immunity 2022;55:527–41.
22. Baban B, Chandler PR, Sharma MD, Pihkala J, Koni PA, Munn DH, et al. IDO activates regulatory T cells and blocks their conversion into Th17-like T cells. J Immunol 2009;183:2475–83.
23. Grohmann U, Fallarino F, Puccetti PT. DCs and tryptophan: much ado about IDO. Trends Immunol 2003;24:242–8.
24. Fallarino F, Grohmann U, You S, McGrath BC, Cavener DR, Vacca C, et al. The combined effects of tryptophan starvation and tryptophan catabolites down-regulate T cell receptor zeta-chain and induce a regulatory phenotype in naive T cells. J Immunol 2006;176:6752–61.
25. Sharma MD, Baban B, Chandler P, Hou D-Y, Singh N, Yagita H, et al. Plasmacytoid dendritic cells from mouse tumor-draining lymph nodes directly activate mature Tregs via indoleamine 2,3-dioxygenase. J Clin Invest 2007;117:2570–82.
26. Spranger S, Spaapen RM, Zha Y, Williams J, Meng Y, Ha TT, et al. Up-regulation of PD-L1, IDO, and T(regs) in the melanoma tumor

microenvironment is driven by $CD8^+$ T cells. Sci Transl Med 2013;5: 200ra116.
27. Cabrita R, Lauss M, Sanna A, Donia M, Skaarup Larsen M, Mitra S, et al. Tertiary lymphoid structures improve immunotherapy and survival in melanoma. Nature 2020;577:561–5.
28. Helmink BA, Reddy SM, Gao J, Zhang S, Basar R, Thakur R, et al. B cells and tertiary lymphoid structures promote immunotherapy response. Nature 2020; 577:549–55.
29. Petitprez F, de Reyniès A, Keung EZ, Chen TW-W, Sun C-M, Calderaro J, et al. B cells are associated with survival and immunotherapy response in sarcoma. Nature 2020;577:556–60.
30. Nakamura M, Magara T, Kano S, Matsubara A, Kato H, Morita A. Tertiary lymphoid structures and chemokine landscape in virus-positive and virus-negative merkel cell carcinoma. Front Oncol 2022;12:811586.
31. Sharma MD, Pacholczyk R, Shi H, Berrong ZJ, Zakharia Y, Greco A, et al. Inhibition of the BTK-IDO-mTOR axis promotes differentiation of monocyte-lineage dendritic cells and enhances anti-tumor T cell immunity. Immunity 2021;54:2354–71.
32. Hellmann MD, Gettinger S, Chow LQM, Gordon M, Awad MM, Cha E, et al. Phase 1 study of epacadostat in combination with atezolizumab for patients with previously treated advanced nonsmall cell lung cancer. Int J Cancer 2020;147: 1963–9.